Journal of Applied Physics ARTICLE scitation.org/journal/jap

On the kinetics of the exchange of hydrogen between hydrogen–boron pairs and hydrogen dimers in crystalline silicon

Cite as: J. Appl. Phys. **131**, 165702 (2022); doi: 10.1063/5.0086307
Submitted: 24 January 2022 · Accepted: 5 April 2022 ·
Published Online: 27 April 2022

Dominic C. Walter,[1,a)] Vladimir V. Voronkov,[2] Robert Falster,[4] Dennis Bredemeier,[1,3] and Jan Schmidt[1,3]

AFFILIATIONS

[1]Institute for Solar Energy Research Hamelin (ISFH), Am Ohrberg 1, 31860, Emmerthal, Germany
[2]Global Wafers, Via Nazionale 59, 39012 Merano, Italy
[3]Department of Solar Energy, Institute of Solid-State Physics, Leibniz University Hannover, Appelstr. 2, 30167 Hanover, Germany
[4]Harrison's Lane, Woodstock, OX20 1SS, UK

[a)]**Author to whom correspondence should be addressed:** d.walter@isfh.de

ABSTRACT

Silicon samples after fast-firing with a hydrogen-rich silicon nitride layer on their surfaces can contain high concentrations of hydrogen (up to 6×10^{15} cm^{-3} in this study). Directly after fast-firing, this hydrogen is mostly present in a neutral dimeric state. Subsequent dark annealing applied in a temperature range between 140 and 175 °C leads to a conversion of dimers into HB pairs, which means that a significant number of boron acceptors are electrically inactive. The concentration of inactive boron, the hydrogen–boron (HB) pair concentration [HB], can thus be determined by measuring the change in specific resistivity before and after annealing. In our study, after the initial anneal for HB pair formation, the same samples are subsequently annealed at stepwise increasing higher temperatures, which leads to a partial backward conversion of HB pairs into neutral hydrogen dimers. This is indicated by a gradual reduction of the resistivity upon increasing the annealing temperature. By measuring the transient curves [HB](t) during each temperature step on samples with different boron content, we extract the parameters for the exchange between the HB pairs and the hydrogen dimers within the framework of our presented physical model. Apart from the backward formation of hydrogen dimers, from HB pairs upon increasing temperature, prolonged annealing at the same temperature leads to a transition of HB pairs into a more stable form of hydrogen dimers, compared to the initial form after fast-firing. This transition is also included in our proposed defect model.

I. INTRODUCTION

The fabrication of silicon solar cells with screen-printed metal contacts[1,2] involves a fast-firing step to form the electrical contacts between the metals and the silicon. In most industrial silicon solar cells, a hydrogen-rich silicon nitride (SiN_x:H) with hydrogen concentrations in the range of 10–20 at. %[3] is present at the surface, which is applied for anti-reflection and surface passivation purposes. During the contact firing step, large amounts of hydrogen can be introduced from the SiN_x:H layer into the silicon bulk,[4–7] where it can significantly affect the recombination properties of defects and hence the solar cell efficiency. It was suspected in several studies[8–10] that hydrogen is vital for permanent recovery of the bulk carrier lifetime in Czochralski-grown silicon after boron–oxygen-related light-induced degradation, a process often referred to as regeneration. However, only very recently, the direct correlation of the hydrogen concentration in the silicon and the regeneration behavior was directly shown, applying the same technique for hydrogen detection as employed in this study.[11] Contrary to the positive impact of hydrogen, it was shown that hydrogen may also cause severe lifetime degradation in silicon materials,[12–14] an effect sometimes referred to as "Light and elevated Temperature Induced Degradation" (LeTID).

During the fast-firing step, cell temperatures in the range of 750–850 °C are reached for a couple of seconds. At these relatively high temperatures, hydrogen is expected to exist in a fast-diffusing atomic form, and it is expected to penetrate through the entire depth of the silicon wafer.[7,15] In this respect, we assume the firing process to be analogous to quenching from high temperature, after

hydrogen saturation of a sample within a hydrogen gas atmosphere.[16,17] In the saturated and quenched samples cooled down to room temperature, hydrogen is known[16,17] to exist mostly in a mobile dimeric form, which can be traced by a weak infrared absorption band, which we labeled H_{2A}.[15] Consequently, we expect the same state of hydrogen, H_{2A}, to be the dominant state in solar cells or lifetime samples directly after the fast-firing process.

Upon dark annealing at around 160 °C, directly subsequent to the fast-firing step, these dimers are converted into HB pairs, which can be detected by a strong IR absorption band at low temperatures.[16] The formation of HB pairs means, vice versa, a partial electrical neutralization of boron acceptors by hydrogen, which could be referred to as "hydrogen passivation" of the boron acceptors. Accordingly, the hole concentration p is reduced to $p = N_B - [\mathrm{HB}]$, with N_B being the total boron concentration and [HB] being the concentration of HB pairs. Hence, a conversion of H_{2A} into HB by dark annealing can be traced in a simple way, just by measuring the sample's resistivity ρ before and after dark annealing, e.g., via an eddy-current measurement[6] or via a four-terminal electrical resistance measurement on evaporated contacts.[18]

In general, the resistivity-based results on fired samples[6] are consistent with the IR-based results on saturated–quenched samples.[16] Compared to the increase in resistivity observed upon dark annealing after fast-firing, the firing process alone does not change the resistivity significantly, which shows that hydrogen is predominantly in the neutral state right after fast-firing, corresponding to H_{2A} according to the above discussion. The subsequent dark annealing can lead to a remarkable increase in resistivity corresponding to the production of HB pairs. Concentrations as high as $3 \times 10^{15}\,\mathrm{cm}^{-3}$ have been observed after fast-firing, applying this method.[6] It is also worth mentioning that the time scale of the HB formation is similar in both resistivity and IR-based results.

In our previously presented model,[15] the rate-limiting step for conversion of H_{2A} into HB is assumed to be a hole-assisted dissociation of dimers: $H_{2A} + h^+ \rightarrow H^+ + H^0$. Subsequent quick steps are recharging H^0 into H^+ by capturing a hole and trapping the H^+ by B^- into neutral HB pairs. Consequently, the overall reaction is

$$H_{2A} + 2h^+ + 2B^- \rightarrow 2HB \tag{1}$$

that removes two holes per each lost dimer. The conversion of H_{2A} into HB is energetically favored due to high binding energy of H^+ and B^-. The kinetic equation for the reversible conversion reads[15]

$$\frac{d[H_{2A}]}{dt} = -(\alpha_1 p + \alpha_0)([H_{2A}] - \chi_A [\mathrm{HB}]^2/(p[B^-])^2). \tag{2}$$

In this equation, χ_A is the equilibrium constant describing the equilibrium between H_{2A} dimers and HB pairs. α_0 and α_1 are dissociation rate coefficients of the two possible dissociation processes of H_{2A}. The total rate coefficient, $(\alpha_1 p + \alpha_0)$, includes the term $\alpha_1 p$ due to reaction (1) as well as α_0, which describes the direct dissociation of H_{2A} into $H^0 + H^0$ that may become important at lower p. Note that for non-compensated material the hole concentration p is identical to $[B^-]$. According to Eq. (2), [HB] tends toward a saturated value that corresponds to the equilibrium between the two species, HB and H_{2A}—when the right-hand part of Eq. (2) equals zero. The saturated concentrations of the two species depend on the value of the equilibrium constant χ_A. Note, we assume an equilibrium reaction, i.e., the formation of HB from H_{2A} as well as the re-formation of H_{2A} to HB occur simultaneously.

In the course of conversion—from H_{2A} to HB and backward—the total boron concentration, $N_B = [B^-] + [\mathrm{HB}]$, and the total hydrogen concentration, $C_H = [\mathrm{HB}] + 2[H_{2A}]$, remain constant. Hence, Eq. (2) gives the time derivative $d[\mathrm{HB}]/dt$ in dependence of only one single variable, [HB].

In the present study, we focus on a detailed study of the time evolution of [HB] for different annealing temperatures and for silicon samples covering a broad range of starting resistivities (i.e., a broad range of boron concentrations N_B). Our experimental approach is thereby to fit the measured transient curves [HB](t) using Eq. (2) and to extract the kinetic parameters α_1 and α_0 as well as the equilibrium constant χ_A as a function of the dark-annealing temperature.

II. EXPERIMENTAL DETAILS

To determine the kinetic parameters as well as the equilibrium constant, we processed boron-doped float-zone silicon samples (FZ-Si) with different base resistivities ranging between 0.51 and 3.15 Ω cm (corresponding to boron concentrations N_B ranging from 4.5×10^{15} to $3.18 \times 10^{16}\,\mathrm{cm}^{-3}$). First, the samples were etched in an aqueous solution of potassium hydroxide several times to ensure comparable thicknesses of the finished samples. After processing, we determined an average thickness of $(158 \pm 6)\,\mu$m. Afterward, the samples underwent a phosphorus diffusion at 820 °C resulting in sheet resistance of the n^+-region of 105 Ω/sq. After the removal of the diffused region, a hydrogen-rich silicon nitride (SiN_x:H) layer was deposited onto both surfaces in a plasma-enhanced chemical vapor deposition (PECVD) process using a PlasmaLab 80+ tool (Oxford instruments). In order to introduce a high hydrogen concentration into the silicon bulk, we chose a refractive index of $n = 2.3$ and a layer thickness of $d = 120$ nm.[13] On two samples with a base resistivity of ∼3 Ω cm (denoted samples 10 and 11), the deposited layer is with $d = 80$ nm thinner and the refractive index with $n = 2.1$ slightly smaller. After sample processing, the base resistivity was determined as stated below. Subsequently, the samples underwent a fast-firing process in an industrial conveyor belt firing furnace (DO-FF-6.300-800, centrotherm) at two different peak temperatures, as typically applied in the industrial production of silicon solar cells. For the first process, we determined the average sample peak temperature during the firing process to be $\vartheta_{\mathrm{peak}} = (820 \pm 15)$ °C and for the second process, an average sample peak temperature of $\vartheta_{\mathrm{peak}} = (755 \pm 15)$ °C was measured using a temperature tracker (DQ1860A from Datapaq).

The resistivity of the samples is measured by applying the eddy-current method using the sample stage of the WCT-120 lifetime tester (Sinton Instruments). Instead of using the standard measurement procedure, we directly measure the output voltage (8845A, Fluke) of the resonant circuit as well as the temperature of the samples on the measurement stage. Using a calibration procedure, we calculate the resistivity of the sample directly from the measured voltages and extrapolate the resistivity to a temperature

of 25 °C. All resistivity values given in the following correspond to the resistivity at 25 °C.[6] In addition, the uncertainties given in the following correspond to the statistical uncertainty as determined via Gaussian error propagation.

III. RESULTS

In the state directly after fast-firing, resistivity ρ_0 is typically slightly higher than ρ_s, the resistivity after sample processing. We attribute this difference to a small amount of HB pairs formed along with the dominant H_{2A} species during the firing process.[18,19] Figure 1 shows the corresponding resistivities of the samples under investigation fired at the measured peak temperature of 820 °C. For two samples, 10 and 11, the resistivity after firing is slightly lower than before firing. Since these two samples feature a different SiN_x:H layer than the other samples (see Experimental section), this may indicate that the hydrogen source already influences the HB pair formation during the firing process. In addition, there is a complicating feature regarding the HB pairs in the as-fired and in the dark-annealed states: as we have shown previously, HB pairs formed during dark annealing are lost again upon illuminated annealing, as suggested by the observed loss in resistivity.[19] In Ref. 19, we attributed this effect to the backward formation of H_{2A} dimers. However, the resistivity is not reduced to the initial value ρ_s but to the as-fired value ρ_0.

It seems that the as-fired HB pairs are more stable—and different from those produced by dark annealing. Since we are studying HB pairs formed upon dark annealing, we use as a reference state the resistivity measured on the as-fired samples rather than the resistivity measured before firing, i.e., in the pre-fired state. Consequently, the HB pair concentration [HB] of the species exchanging with H_{2A} is then set to zero for the as-fired samples.

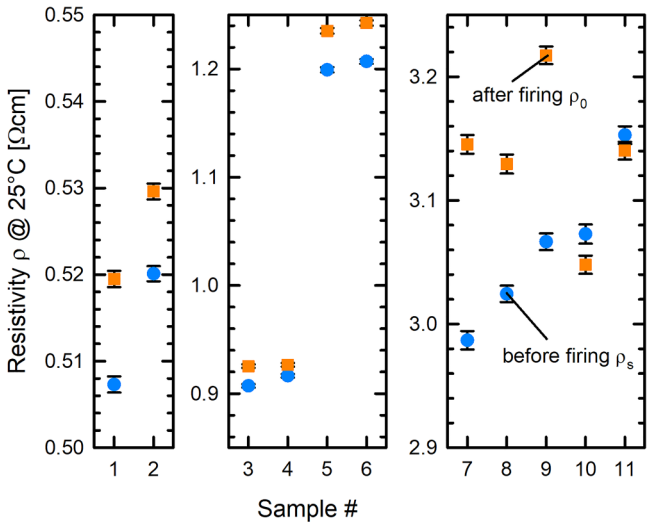

FIG. 1. Resistivities of the samples under investigation measured before firing ρ_s and after firing ρ_0 at a measured peak temperature of 820 °C.

The hole concentration $p(t)$—determined from the current value of the resistivity—is equal to $(N_B - [HB])$ for a non-compensated material. As explained above, the total boron concentration N_B is set to the hole concentration p_0 in the as-fired state. Our quantity of interest, the HB pair concentration [HB] is then calculated according to

$$[HB] = p_0 - p(t). \quad (3)$$

If the reference state of zero [HB] were chosen to be the pre-fired state, then p_0 in Eq. (3) would be replaced with the value p_s (for the pre-fired sample). We tried both options for the reference state but adopt the former one (referenced to p_0), which gives a better fit to our experimental data. Please note that the extracted model parameters are very similar for both options.

The rate of conversion from H_{2A} to HB is reduced at a lower T.[6,15] Due to the slow formation process, the lowest temperature still suitable for tracing the conversion was chosen to be 140 °C. In this case, the required time scale of annealing to reach saturation is in the range of 500 h. In order to deduce the temperature dependence of the equilibrium constant χ_A, the samples which were previously annealed at 140 °C up to saturation of the resistivity (i.e., to saturation of the HB pair concentration) were subsequently annealed again, at sequentially increasing temperatures up to a maximum temperature of 270 °C. During each annealing step, the change in resistivity was monitored to ensure that the temperature-dependent saturation value was reached.

A. Initial annealing at 140 °C in darkness

In Fig. 2, the change of the HB pair concentration upon dark annealing at 140 °C is shown, separately for samples of a higher boron concentration N_B, i.e., low resistivity [Fig. 2(a)] and for samples of a lower boron concentration, i.e., high resistivity [Fig. 2(b)].

In all cases, the HB pair concentration reaches a saturated value; however, there is a qualitative difference between these two groups of samples. Setting the right-hand term of Eq. (2) to zero, the saturated concentration of H_{2A} dimers can be expressed as

$$[H_{2A}] = \chi_A [HB]^2/(N_B - [HB])^4. \quad (4)$$

Consequently, due to the high exponent in the denominator, it is highly sensitive with respect to the absolute value of the doping concentration N_B.

With the values of the equilibrium constant χ_A estimated below, the remaining amount of H_{2A} is negligible at $N_B > 10^{16}$ cm^{-3}. In this case, the HB pair concentration approaches the total hydrogen concentration C_H. As a consequence, the solution of the kinetic equation [Eq. (2)] is only sensitive to the kinetic parameters α_1 and α_0 but not to the value of the equilibrium constant χ_A.

A good fit is obtained neglecting the term α_0, suggesting that the dissociation of hydrogen dimers proceeds predominantly via a hole-assisted process. For the samples with doping concertation $N_B > 10^{16}$ cm^{-3}, i.e., with resistivities 0.53 Ω cm (no. 2), 0.93 Ω cm (no. 3), 1.24 Ω cm (samples no. 5 and no. 6), the fitted coefficient

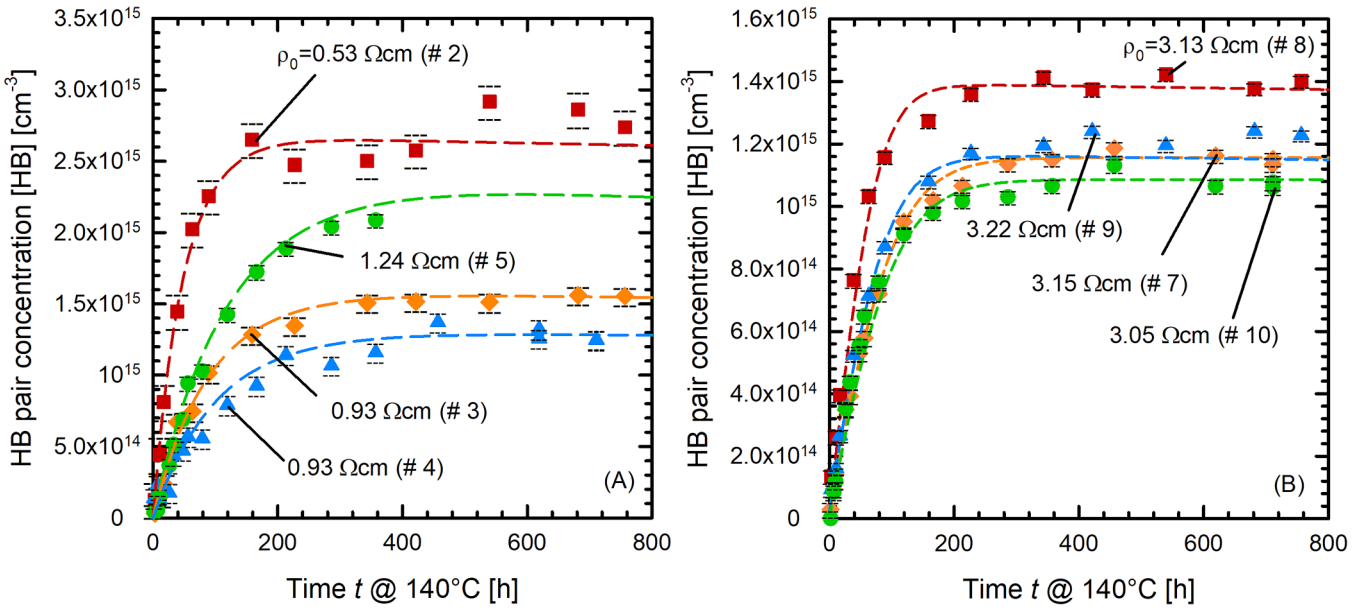

FIG. 2. The formation of HB pairs by dark annealing at 140 °C (a) for samples with low base resistivity ρ_s (ranging from 0.53 to 1.24 Ω cm) and (b) for samples with high base resistivity (ranging from 3.05 to 3.22 Ω cm). The dashed curves are calculated using Eq. (2) with best-fit parameters.

is $\alpha_1 = (2.1 \pm 0.3) \times 10^{-22}$ cm^3/s and somewhat smaller $\alpha_1 = (1.3 \pm 0.6) \times 10^{-22}$ cm^3/s for the other two samples with resistivities of 0.52 Ω cm (no. 1) and 0.93 Ω cm (no. 4). The total hydrogen concentration C_H, almost identical to the plateau value of [HB], is in a range of (1.25 to 2.7) $\times 10^{15}$ cm^{-3}.

With a specified value for $\alpha_1 = 2.1 \times 10^{-22}$ cm^3/s, the computed curves for the second group of samples [$N_B < 10^{16}$ cm^{-3}, Fig. 2(b)] depend on two fitting parameters: the equilibrium constant χ_A and the total hydrogen concentration C_H. In this case, the saturation value of the HB pair concentration [HB] is only a fraction of the total hydrogen concentration C_H, since, according to Eq. (4), the remaining H_{2A} concentration at lower doping concentrations N_B is not negligible in contrast to the samples shown in Fig. 2(a) with higher doping concentrations.

In total, there were eight samples, four of which are shown in Fig. 2(b). The fitted values of the equilibrium constant χ_A are between 0.09×10^{48} and 0.24×10^{48} cm^{-6}, with an average value of $(0.15 \pm 0.05) \times 10^{48}$ cm^{-6}. The fitted values of C_H are in the range of (2.5 to 6.5) $\times 10^{15}$ cm^{-3}—overlapping with the range found above for the lower-resistivity samples.

B. Subsequent anneals at higher temperatures

Figure 3 shows the evolution in the resistivity of one single sample upon subsequent annealing at increasing temperatures from 150 to 250 °C [sample no. 8, $\rho_0 = 3.13$ Ω cm, in Fig. 2(b)]. For each annealing temperature, we observe a decrease in the sample's resistivity. Apart from the saturation value, also the time span

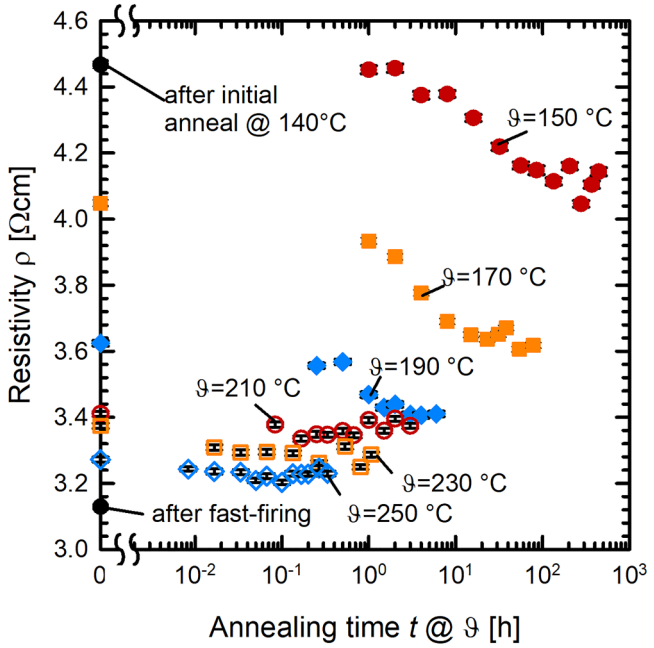

FIG. 3. Resistivity ρ of one single sample with a starting resistivity of 3.13 Ω cm (no. 8) upon subsequent annealing steps from 150 up to 250 °C. Black circles indicate the resistivity measured directly after fast-firing as well as after the initial HB pair formation at 140 °C.

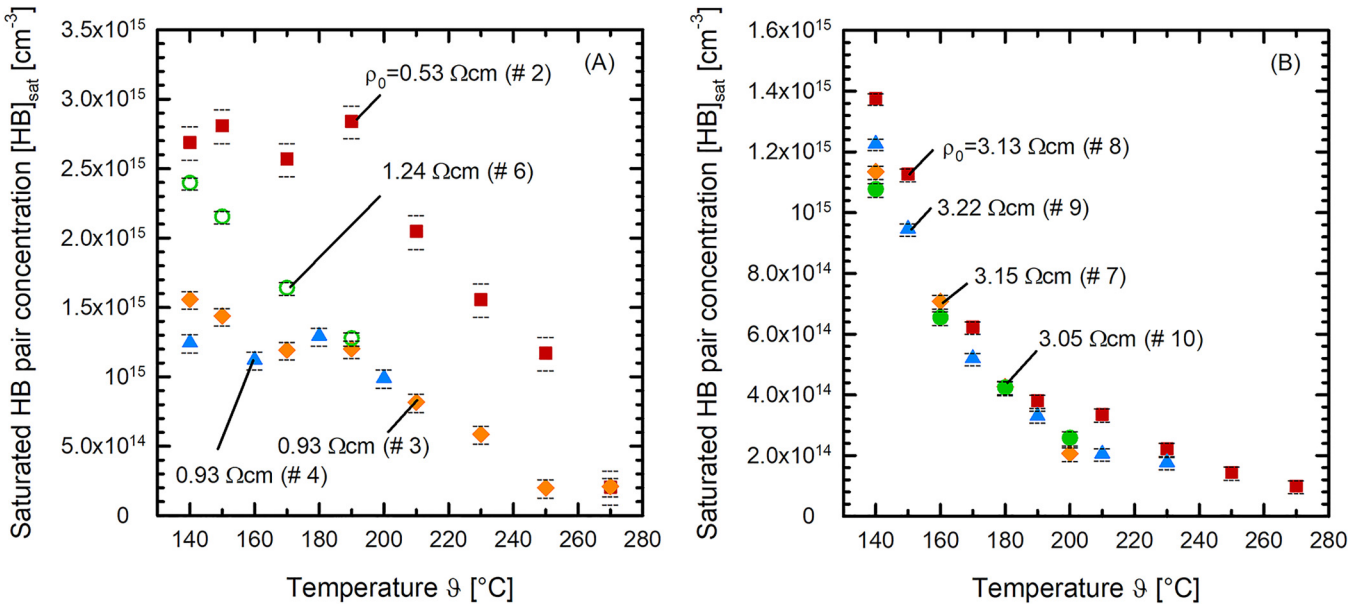

FIG. 4. Saturated HB pair concentration $[HB]_{sat}$ of low resistivity samples (a) and high resistivity samples (b). For samples with base resistivities $<1\ \Omega$ cm, $[HB]_{sat}$ remains constant up to 190 °C before it starts to decrease, while for samples with base resistivities $>1\ \Omega$ cm, $[HB]_{sat}$ strongly decreases for all temperatures above 140 °C.

necessary to reach the saturation value decreases strongly with increasing temperature. Both observations indicate that the equilibrium constant χ_A and the kinetic parameter α_1 depend critically on the annealing temperature.

Figure 4 summarizes the determined saturation values $[HB]_{sat}$ of the samples under investigation, in Fig. 4(a) for the low resistivity samples and in Fig. 4(b) for the high resistivity samples. Interestingly, for the low resistivity samples ($<1\ \Omega$ cm), we observe almost constant saturation values up to an annealing temperature of 190 °C.

Above this temperature, the saturation values start to decrease with increasing temperature. This further supports the assumption that for low resistivity samples at low temperatures, the saturated value of HB is determined by the total hydrogen concentration and is not affected by the equilibrium constant χ_A. For high resistivity samples, see Fig. 4(b), the saturation values decrease for all investigated temperatures above 140 °C.

For all the samples annealed up to saturation at 140 °C, the total hydrogen concentration C_H has been determined above. According to Eq. (4), an increased equilibrium constant χ_A will result in a larger saturated concentration $[H_{2A}]$ and, accordingly, in a smaller saturated $[HB]_{sat}$, i.e., a reduction in resistivity (see Fig. 3). Using Eq. (4), the equilibrium constant can be expressed through the total hydrogen concentration C_H and the new saturated value of $[HB]_{sat}$,

$$\chi_A = 0.5(C_H - [HB]_{sat})(N_B - [HB]_{sat})^4/[HB]^2_{sat}. \quad (5)$$

The saturated $[HB]_{sat}$ for our performed sequential anneals on the samples under investigation is shown in Fig. 5. The data are for the low resistivity samples, corresponding to samples no. 2, no. 3, and no. 5 in Fig. 2(a). Reliable values of χ_A can only be obtained if both, $[HB]_{sat}$ and $C_H - [HB]_{sat}$, in Eq. (5) are significantly larger than the scatter in [HB].

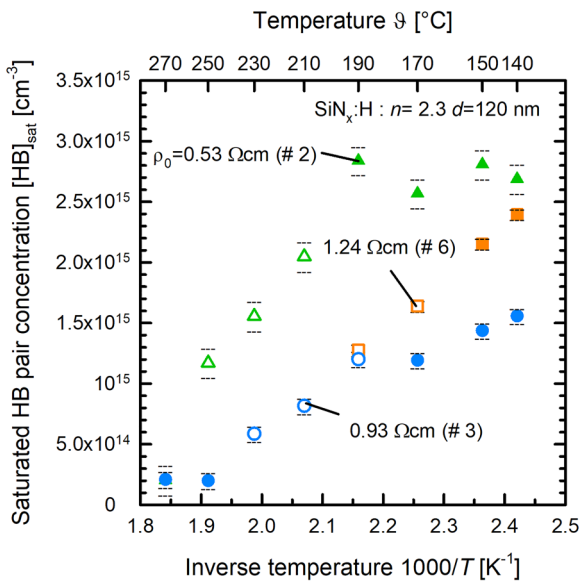

FIG. 5. Saturated concentration of HB pairs by sequential anneals of samples with base resistivities of $\rho_s = 0.53$ (no. 2), $\rho_s = 0.93$ (no. 3), and $\rho_s = 1.24\ \Omega$ cm (no. 5) with a higher boron concentration.

TABLE I. Equilibrium constants χ_A determined from Fig. 5.

Resistivity ρ_0 (Ω cm)	Temperature (°C)	Equilibrium constant χ_A ($cm^3\ s^{-1}$)	Upper boundary	Lower boundary
0.53	210	5.38×10^{49}	8.54×10^{49}	2.94×10^{49}
0.53	230	1.75×10^{50}	2.55×10^{50}	1.16×10^{50}
0.53	250	4.35×10^{50}	6.41×10^{50}	2.94×10^{50}
0.93	190	6.41×10^{48}	9.92×10^{48}	3.63×10^{48}
0.93	210	3.22×10^{49}	4.56×10^{49}	2.23×10^{49}
0.93	230	8.69×10^{49}	1.26×10^{50}	6.02×10^{49}
1.24	170	1.55×10^{48}	1.89×10^{48}	1.26×10^{48}
1.24	190	4.35×10^{48}	5.21×10^{48}	3.62×10^{48}

The points used to determine χ_A are marked by open symbols in Fig. 5. The values deduced from these points are summarized in Table I. Considering the uncertainties involved in the measurements, the deduced values agree very well at specific temperatures.

For the samples of lower boron concentration N_B (i.e., samples no. 7–no. 11), the same procedure is not so straightforward since the total hydrogen concentration C_H is less certain: it depends on the adopted value of the kinetic coefficient α_1. For example, a transient curve for annealing at 170 °C, after the preceding anneals at 140 and 150 °C, is shown in Fig. 6(a).

The total hydrogen concentration determined initially from the annealing at 140 °C for this sample is $C_H = 7.0 \times 10^{15}\ cm^{-3}$ together with the dissociation rate coefficient $\alpha_1 = 2.1 \times 10^{-22}\ cm^3/s$. The parameters, deduced by fitting the transient curve in Fig. 6(a) using Eq. (2), are $\chi_A = (1.65 \pm 0.25) \times 10^{48}\ cm^{-6}$ and $\alpha_1 = (5.0 \pm 1.0) \times 10^{-22}\ cm^3/s$ for the annealing temperature of 170 °C. The values deduced for other temperatures (150 and 190 °C) are less reliable due to a larger scatter in [HB](t). They will be displayed later, in the Discussion section.

For the sample corresponding to the curve shown in Fig. 6(b), the previously determined total hydrogen concentration is $C_H = 3.5 \times 10^{15}\ cm^{-3}$. For the decay shown during the anneal at 160 °C, we deduced the parameters $\chi_A = (0.55 \pm 0.1) \times 10^{48}\ cm^{-6}$ and $\alpha_1 = (6.5 \pm 1.5) \times 10^{-22}$.

C. Prolonged annealing at a constant temperature of 175 °C

Apart from the investigations above, another set of five samples was fired at a lower measured peak temperature of (755 ± 15) °C. Directly after firing, the samples were annealed in darkness at an annealing temperature of 175 °C, arbitrarily chosen within the temperature range for HB pair formation. The resistivities of these samples measured after firing ranged between $\rho_0 = 0.52$ and 3.01 Ω cm. Figure 7(left) shows the measured change in resistivity upon this dark anneal. For all samples, we observe an increase in resistivity followed by a decrease upon prolonged annealing. The [HB](t) curves of two of these samples with starting resistivities of 1.24 and 3.01 Ω cm are shown exemplarily in Fig. 7 (right) together with the computed curves (solid lines) according to our model.

The concentration [HB] quickly reaches a maximum in a shorter time span compared to the time needed to reach the saturation in Fig. 3 for the 170 °C annealing temperature and then slowly

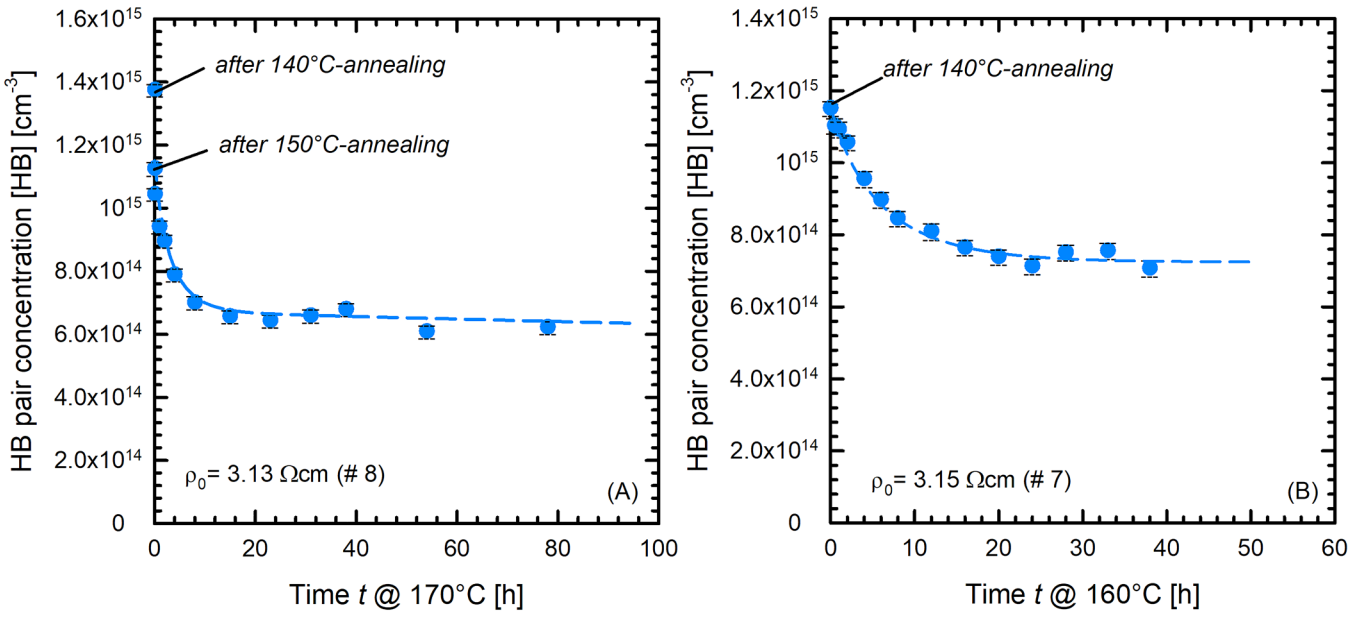

FIG. 6. Loss in HB pair concentration upon additional annealing following the initial anneal at 140 °C (a) at an annealing temperature of 170 °C, after an anneal at 150 °C in between and (b) at an annealing temperature of 160 °C. The dashed lines are calculated according to our model.

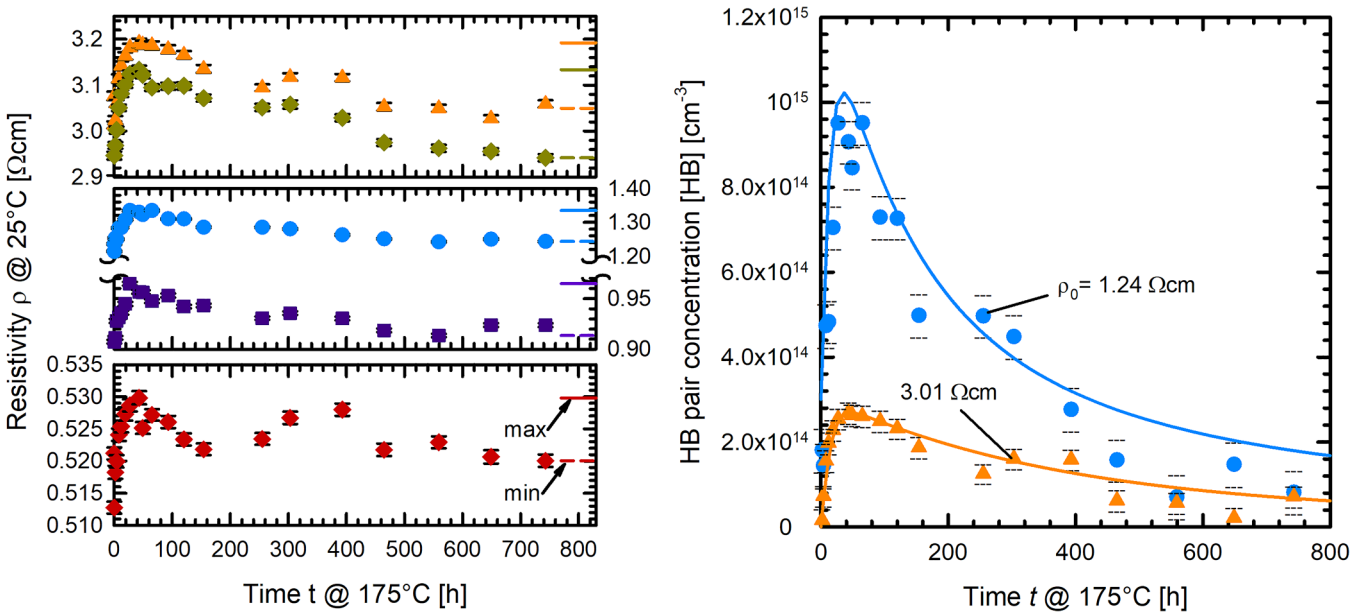

FIG. 7. Left: change in resistivity ρ upon annealing at 175 °C in darkness directly after fast-firing. Maximum and minimum values are highlighted by solid and dashed lines, respectively. Right: evolution of [HB] by prolonged annealing at 175 °C. The curves correspond to samples with a starting resistivity $\rho_0 = 1.24$ Ω cm (blue circles) and 3.01 Ω cm (orange triangles). The computed curves (solid lines) take a loss of hydrogen species into account. HB pairs and H_{2A} dimers are lost while simultaneously stable dimers H_{2C} are produced.

decreases. A slow loss of HB upon prolonged annealing is similar to that reported in Ref. 20 for saturated/quenched samples. This behavior could be attributed[15] to the formation of stable dimers H_{2C} of a different configuration than H_{2A} by a pairing reaction $HB + H^+ \rightarrow H_{2C} + B^- + 2h^+$ at a rate

$$\frac{d[H_{2C}]}{dt} = \beta[HB]^2/[B^-]. \quad (6)$$

The concentration of HB accordingly decreases at a rate $-2\,\beta\,[HB]^2/[B^-]$, since two HB pairs are lost in order to form one single H_{2C} dimer.

The loss of [HB] is not well reproduced just by Eq. (6) using a single value for the pairing coefficient, β. However, a good fit is achieved if there is an additional path of H_{2C} formation—by direct reconfiguration of H_{2A} into H_{2C},

$$\frac{d[H_{2C}]}{dt} = \beta^{\dagger}[H_{2A}]. \quad (7)$$

The concentration of H_{2A} accordingly decreases at a rate $-\beta^{\dagger}[H_{2A}]$ since one H_{2A} dimer is lost to form a single H_{2C} dimer.

The total time derivative of [HB] is hence obtained from combining Eqs. (2) and (6). The total time derivative of $[H_{2A}]$ is obtained by combining Eqs. (2) and (7).

The computed [HB](t) curves for the five inspected samples reproduce the measured ones for the assumed parameters summarized in Table II. The total concentration C_H, determined individually for each curve, varies for these samples in a range from 1×10^{15} to 1.8×10^{15} cm^{-3}.

Note that, within the assumption of our model, in the previous cases shown in Fig. 2, the duration of the anneal was not long enough to resolve the loss of HB due to the formation of H_{2C}.

D. Prolonged annealing at a constant temperature of 160 °C

Finally, we also continued the annealing of samples from our previous study[6] for longer annealing times at 160 °C to investigate the subsequent decrease in resistivity upon reaching the maximum.

In Fig. 8, the resistivity as well as the change in HB pair concentration is shown for two samples with different SiN_x:H layers as

TABLE II. Fit parameters used to describe formation and disappearance of HB pairs shown in Fig. 7.

Parameter	Value
Dissociation rate coefficient α_1 ($\times 10^{-22}$ cm^3/s)	10 (set from estimation above)
Equilibrium constant χ_A ($\times 10^{48}$ cm^{-6})	2 (set from estimation above)
Pairing rate coefficient β (s^{-1})	10^{-5}
Reconfiguration rate coefficient $\beta^{\dagger}$ (s^{-1})	1.3×10^{-6}

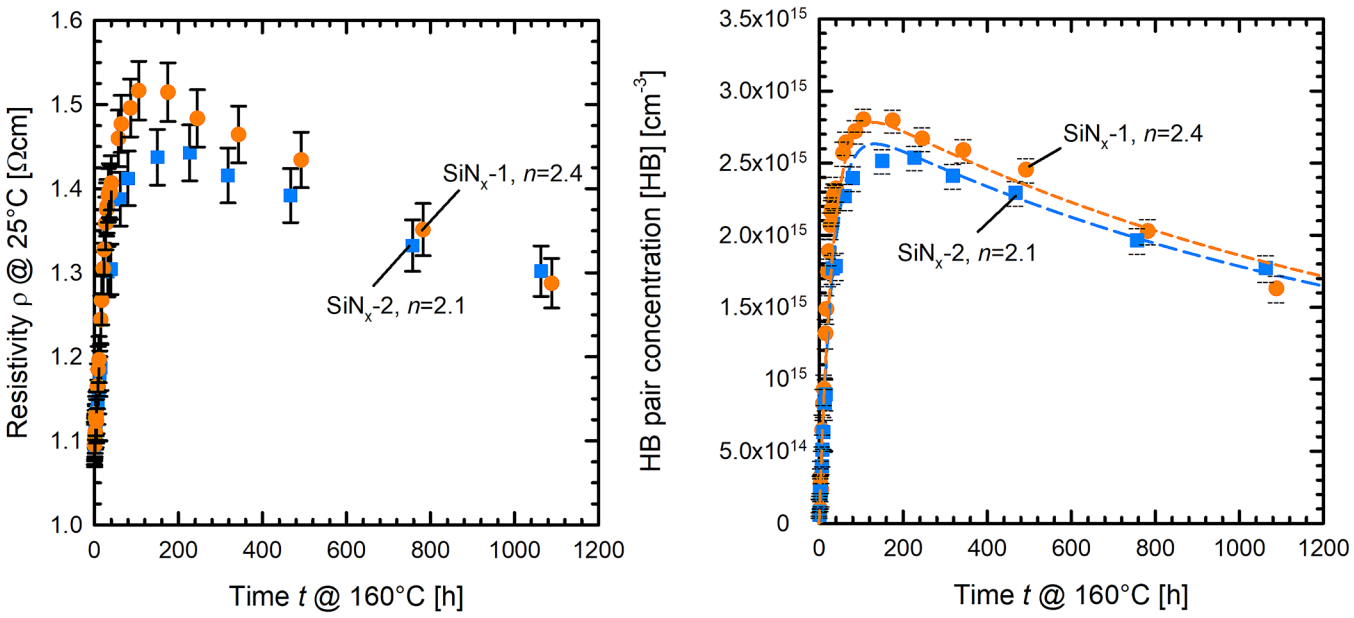

FIG. 8. Long-time evolution of resistivity (left) and HB pair concentration (right) by prolonged annealing at 160 °C. Dashed lines are the best fit to the data with a total hydrogen concentration of $C_H = 3.8 \times 10^{15}$ cm^{-3} (orange curve) and $C_H = 3.5 \times 10^{15}$ cm^{-3} (blue curve).

hydrogen source, denoted SiN_x–1 and SiN_x–2, which slightly differ in their refractive index with $n = 2.4$ and $n = 2.1$, respectively (more details can be found in Ref. 6). Again, as observed before, upon prolonged annealing at 160 °C, the resistivity increases within the first 200 h before the resistivity decreases again, on a longer time scale. Consequently, as can be seen in Fig. 8 (right), a prolonged anneal leads to a loss of HB pairs, just like in the preceding case of the 175 °C anneal. If the equilibrium constant is set to the value estimated above, $\chi_A = 0.55 \times 10^{48}$ cm^{-6}, then, the best-fit parameters for the rising part of the curves are $\alpha_1 = (5 \pm 1) \times 10^{-22}$ cm^3/s and $C_H = (3.8 \pm 0.1) \times 10^{15}$ cm^{-3} for the SiN_x–1 curve and $\alpha_1 = (4.5 \pm 1) \times 10^{-22}$ cm^3/s and $C_H = (3.5 \pm 0.1) \times 10^{15}$ cm^{-3} for the SiN_x-2 curve. For the subsequent decay, the parameters are set to $\beta = 4.5 \times 10^{-7}$ and $\beta^{\dagger} = 10^{-7}$ s^{-1}, for both curves. Please note that due to the newly determined value for the equilibrium constant χ_A, the total hydrogen concentration is about 1×10^{15} cm^{-3} higher than the values determined previously,[6] clearly emphasizing the importance of χ_A for an accurate determination of C_H.

IV. DISCUSSION

The most important parameter for the conversion between H_{2A} dimers and HB pairs is the equilibrium constant χ_A. All the values extracted above in the range of 140 to 270 °C are collected in Fig. 9.

The scatter in the data points is reasonably small, and the $\chi_A(T)$ dependence can be well described by a single Arrhenius-type

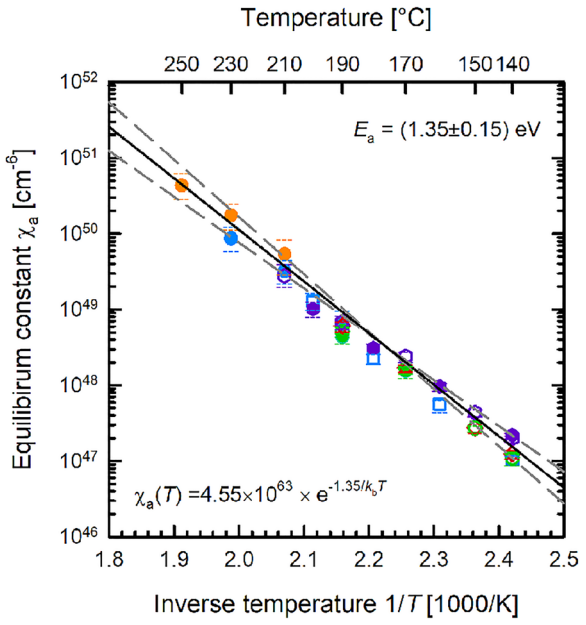

FIG. 9. The equilibrium constant χ_A extracted by dark annealing of the samples under investigation at various temperatures. Different symbols indicate different samples ranging from 0.53 to 3.14 Ω cm in base resistivity after fast-firing. The solid line is a calculated temperature dependence according to an Arrhenius-type dependence as displayed in the plot. Taking the uncertainties into account, we determine activation energy of $E_A = (1.35 \pm 0.15)$ eV.

dependence of the form

$$\chi_A(T) = 4.55 \times 10^{63}\big|_{9.52\times10^{61}}^{2.19\times10^{65}} \times \exp\left(-\frac{1.35\big|_{1.2}^{1.5}}{(k_b T)}\right)(\mathrm{cm}^{-6}). \quad (8)$$

With the Boltzmann constant k_b and activation energy of $E_A = (1.35 \pm 0.15)$ eV. The upper and the lower numbers in the equation indicate the maximum range of the prefactor and the activation energy determined from our data.

The value of E_A may be affected by a neglected formation of stable dimers H_{2C} that was evident for prolonged anneals (see Figs. 7 and 8) but was hard to detect for shorter anneals (see Figs. 2 and 6). Due to the formation of H_{2C}, the total concentration C_H contained in H_{2A} and HB will be progressively decreased by applying numerous sequential anneals, after the 140 °C initial anneal.

To verify this assumption, we subjected a sample with a base resistivity of 3.13 Ω cm (sample no. 8) to a final annealing step at 140 °C, after the seven sequential anneals between 150 and 270 °C. The reduction of the saturation value of the HB pair concentration, corresponding to a reduced total hydrogen concentration C_H is shown in Fig. 10. The dashed curves are computed for the same values of the parameters: $\chi_A = 0.125 \times 10^{48}$ cm^{-6} and $\alpha_1 = 2.13 \times 10^{-22}$ cm^3/s. The deduced hydrogen concentration C_H is $(6.5 \pm 0.5) \times 10^{15}$ cm^{-3} for the initial anneal (orange curve) and $(3 \pm 0.2) \times 10^{15}$ cm^{-3} in the re-annealed sample (blue curve). This means that approximately half of the hydrogen was lost during the annealing sequence, most likely to stable H_{2C} dimers. If a progressive reduction in C_H upon sequential anneals is considered, then the values of the equilibrium constant χ_A deduced from Eq. (5) will be progressively smaller upon raising ϑ, in comparison to those shown in Fig. 9.

A value of the equilibrium constant χ_A at 160 °C has been determined[15] for the saturated concentration of H_{2A} dimers and HB pairs obtained from infrared absorption measurements to be $\chi_A(160\,^\circ C) = 0.04 \times 10^{48}$ cm^{-6}. This number is in a striking discrepancy with the present data (Fig. 9), which shows a significantly larger value of 0.9×10^{48} cm^{-6}. An evident explanation is that the IR calibration[16] for the concentrations of [H_{2A}] and [HB] was not quite accurate. The IR-based concentrations are reconciled with our value, $\chi_A(160\,^\circ C) = 0.9 \times 10^{48}$ cm^{-6}, if the calibration factors for both [HB] and [H_{2A}] are multiplied by a correction factor of 0.5. In other words, the discrepancy could be resolved if we assume that the actual concentrations of HB and H_{2A} in Ref. 16 are about half as low as the reported ones.

The kinetic coefficient α_1 defines, for a specified equilibrium constant χ_A, a specified boron concentration N_B and a specified hydrogen concentration C_H, the time scale of the conversion between hydrogen dimers H_{2A} and HB pairs. The deduced values from the samples under investigation are shown in Fig. 11. The data show a remarkable scatter. Roughly, the temperature dependence can be described in average by an Arrhenius-type temperature dependence with an activation energy of (0.84 ± 0.17) eV, as shown by the solid line in Fig. 11.

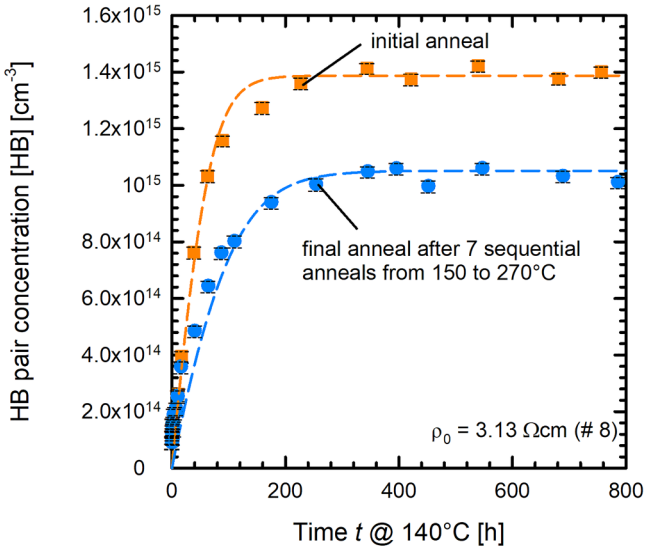

FIG. 10. Evolution of HB pair concentration [HB] at 140 °C for a sample with a base resistivity of 3.13 Ω cm. Orange curve: first anneal at 140 °C directly after firing. Blue curve: last anneal at 140 °C after numerous subsequent annealing steps up to 270 °C. The dashed curves are calculated according to our model.

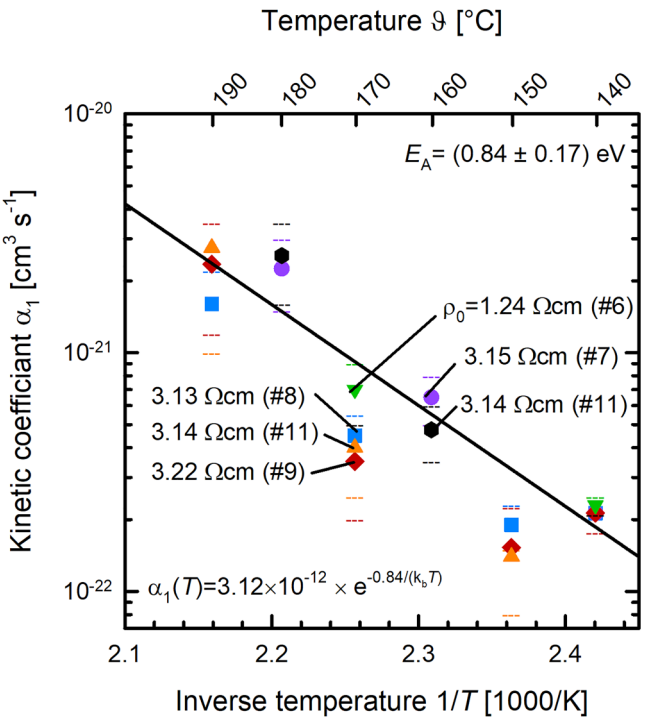

FIG. 11. The kinetic coefficient α_1 extracted by dark annealing of many samples of different boron concentrations N_B, indicated by differently colored symbols at various temperatures. The solid line is a calculated temperature dependence according to an Arrhenius-type dependence, as depicted in the plot, with an activation energy of $E_A = (0.84 \pm 0.17)$ eV.

Another important conclusion of the present work is that the hydrogen concentration C_H introduced by firing widely scatters, from 1×10^{15} to $6.5 \times 10^{15}\,cm^{-3}$, even for the same firing conditions. This, in turn, means that the solubility of hydrogen in silicon is strongly sensitive to the properties of the hydrogen source, in our study, the SiN_x:H layer.

V. SUMMARY

Within this contribution, we have studied the formation of hydrogen–boron pairs (HB pairs) upon dark annealing after introducing hydrogen into the silicon bulk from a hydrogen-rich silicon nitride layer using a fast-firing process. The study comprised boron-doped float-zone silicon samples with base resistivities ranging from 0.51 to 3.2 Ω cm. Our measurements confirmed that while dark annealing at temperatures around 160 °C leads to an increase in the resistivity of the silicon wafers, in the beginning, prolonged annealing at the same temperature leads to a subsequent decrease in resistivity. We attribute this observation to a transition of the dominant state of hydrogen from weakly bound hydrogen dimers H_{2A} to HB pairs at the beginning of the annealing sequence to a transition from the formed HB pairs to more stable hydrogen dimers H_{2C} with different configuration and binding energy than H_{2A} upon prolonged annealing at the same temperature. Furthermore, we have introduced a physical model which allows us to describe the observed behavior. The model uses three main parameters: The kinetic coefficient α_1, describing the transient behavior at the beginning of the annealing sequence, the equilibrium constant χ_A, describing the equilibrium between the H_{2A} dimers and the HB pairs, and the pairing coefficient β, describing the formation of H_{2C} dimers from HB pairs. By subsequently varying the annealing temperature on the same samples, i.e., with a constant hydrogen concentration, we were able to show that both the kinetic coefficient α_1 as well as the equilibrium constant χ_A depend critically on the annealing temperature. In both cases, we measured an Arrhenius-type temperature dependence with an activation energy of (0.84 ± 0.17) eV for the kinetic coefficient α_1 and activation energy of (1.35 ± 0.15) eV for the equilibrium constant χ_A. Knowing the temperature dependence of these parameters is a vital part to determine the total hydrogen concentration accurately from the measured HB pair concentration.

AUTHOR DECLARATIONS

Conflict of Interest

The authors have no conflicts to disclose.

DATA AVAILABILITY

The data that support the findings of this study are available from the corresponding author upon reasonable request.

ACKNOWLEDGEMENTS

D. C. Walter, D. Bredemeier and J. Schmidt acknowledge the financial support by the German State of Lower Saxony.

REFERENCES

[1]L. Frisson, Ph. Lauwers, R. Mertens, R. van Overstraeten, and R. Govaerts, "Screen printed metallization of silicon solar cells," ElectroComp. Sci. Technol. **7**, 107–111 (1980).
[2]R. Preu, E. Lohmüller, S. Lohmüller, P. Saint-Cast, and J. M. Greulich, "Passivated emitter and rear cell—Devices, technology, and modeling," Appl. Phys. Rev. **7**, 041315 (2020).
[3]B. Lenkeit, "Elektronische und strukturelle Eigenschaften von Plasma-Siliziumnitrid zur Oberflächenpassivierung von siebgedruckten, bifacialen silizium-solarzellen," Ph.D. thesis (Hannover, 2002).
[4]F. Jiang, M. Stavola, A. Rohatgi, D. Kim, J. Holt, H. Atwater, and J. Kalejs, "Hydrogenation of Si from SiNx(H) films: Characterization of H introduced into the Si," Appl. Phys. Lett. **83**, 931–933 (2003).
[5]G. Hahn, D. Karg, A. Schonecker, A. R. Burgers, R. Ginige, and K. Cherkaoui, "Kinetics of hydrogenation and interaction with oxygen in crystalline silicon," in *Conference Record of the Thirty-First IEEE Photovoltaic Specialists Conference*, 3–7 January 2005, Lake buena Vista, FL (IEEE, 2005), pp. 1035–1038.
[6]D. C. Walter, D. Bredemeier, R. Falster, V. V. Voronkov, and J. Schmidt, "Easy-to-apply methodology to measure the hydrogen concentration in boron-doped crystalline silicon," Sol. Energy Mater. Sol. Cells **200**, 109970 (2019).
[7]M. Sheoran, D. S. Kim, A. Rohatgi, H. F. W. Dekkers, G. Beaucarne, M. Young, and S. Asher, "Hydrogen diffusion in silicon from plasma-enhanced chemical vapor deposited silicon nitride film at high temperature," Appl. Phys. Lett. **92**, 172107 (2008).
[8]K. A. Münzer, "Hydrogenated silicon nitride for regeneration of light induced degradation," in *Proceedings of. 24th EUPVSEC, Hamburg* (WIP-Munich, 2009), p. 1558–1561.
[9]S. Wilking, A. Herguth, and G. Hahn, "Influence of hydrogen on the regeneration of boron-oxygen related defects in crystalline silicon," J. Appl. Phys. **113**, 194503 (2013).
[10]B. J. Hallam, S. R. Wenham, P. G. Hamer, M. D. Abbott, A. Sugianto, C. E. Chan, A. M. Wenham, M. G. Eadie, and G. Xu, "Hydrogen passivation of B-O defects in Czochralski silicon," Energy Procedia **38**, 561–570 (2013).
[11]L. Helmich, D. C. Walter, R. Falster, V. V. Voronkov, and J. Schmidt, "Impact of hydrogen on the boron-oxygen-related lifetime degradation and regeneration kinetics in crystalline silicon," Sol. Energy Mater. Sol. Cells **232**, 111340 (2021).
[12]D. Bredemeier, D. Walter, S. Herlufsen, and J. Schmidt, "Lifetime degradation and regeneration in multicrystalline silicon under illumination at elevated temperature," AIP Adv. **6**, 035119 (2016).
[13]D. Bredemeier, D. C. Walter, R. Heller, and J. Schmidt, "Impact of hydrogen-rich silicon nitride material properties on light-induced lifetime degradation in multicrystalline silicon," Phys. Status Solidi RRL **13**, 1900201 (2019).
[14]M. Winter, D. Walter, and J. Schmidt, "Carrier lifetime degradation and regeneration in gallium- and boron-doped monocrystalline silicon materials," IEEE J. Photovolt. **11**, 866–872 (2021).
[15]V. V. Voronkov and R. Falster, "Formation, dissociation, and diffusion of various hydrogen dimers in silicon," Phys. Status Solidi B **254**, 1600779 (2017).
[16]R. E. Pritchard, J. H. Tucker, R. C. Newman, and E. C. Lightowlers, "Hydrogen molecules in boron-doped crystalline silicon," Semicond. Sci. Technol. **14**, 77 (1999).
[17]R. E. Pritchard, M. J. Ashwin, J. H. Tucker, and R. C. Newman, "Isolated interstitial hydrogen molecules in hydrogenated crystalline silicon," Phys. Rev. B **57**, R15048–R15051 (1998).
[18]C. Winter, J. Simon, and A. Herguth, "Study on boron–hydrogen pairs in bare and passivated float-zone silicon wafers," Phys. Status Solidi A **218**, 2100220 (2021).
[19]D. C. Walter, D. Bredemeier, R. Falster, V. V. Voronkov, and J. Schmidt, "Disappearance of hydrogen-boron-pairs in silicon during illumination and its relevance to lifetime degradation and regeneration effects in solar cells," in *37th European Photovoltaic Solar Energy Conference and Exhibition* (WIP-Munich, 2020), pp. 140–144.
[20]M. J. Binns, R. C. Newman, S. A. McQuaid, and E. C. Lightowlers, "Hydrogen solubility and defects in silicon," Mater. Sci. Forum **143-147**, 861–866 (1993).